How Stable Are 2H-MoS 2 Edges under Hydrogen Evolution Reaction Conditions?

Nawras Abidi, Audrey Bonduelle-Skrzypczak, Stephan N. Steinmann

How Stable are 2H-MoS_2 Edges under Hydrogen Evolution Reaction Conditions?

Nawras Abidi,[†] Audrey Bonduelle-Skrzypczak,[‡] and Stephan N. Steinmann[*,†]

†*Univ Lyon, Ens de Lyon, CNRS UMR 5182, Université Claude Bernard Lyon 1, Laboratoire de Chimie, F69342, Lyon, France*

‡*IFP Energies nouvelles, Rond-point de l'échangeur de Solaize, 69360 Solaize, France*

E-mail: stephan.steinmann@ens-lyon.fr

Phone: (+33)4 72 72 81 55

Abstract

Transition metal dichalcogenides (TMDs), especially MoS_2, have emerged as a promising class of electrocatalysts for the production of H_2 via the hydrogen evolution reaction (HER) in acidic conditions. The edges of MoS_2 are known for their HER activity, but their precise atomistic nature and stability under HER conditions is not yet known. In contrast to other typical uses of MoS_2 as a catalyst, under HER there is no external source of sulfur. Therefore, the sulfidation of the edges can only decrease under operating conditions and the thermodynamics of the process are somewhat ill-defined. Our results suggest that the 50%S S-edge may be active for HER via the Volmer-Tafel mechanism and is, despite a high H coverage, stable with respect to H_2S release. At the 50%S Mo-edge, the adsorbed hydrogen opens the way for H_2S release, leading to the 0%S Mo-edge, which was previously investigated and found to be HER active. HER being a water-based process, we also considered the effect of the presence of H_2O and the in-situ formation of OH. For the 50%S Mo-edge, H_2O is only very weakly adsorbed and OH formation is unfavorable. Nevertheless, OH assists the loss of sulfur coverage, leading to OH-based HER active sites. In contrast, OH is strongly adsorbed on the 50%S S-edge. By explicitly considering the electrochemical potential using grand-canonical density functional theory, we unveil that the Volmer-Heyrovsky mechanism on sulfur sites is still accessible in the presence of surface OH at the 50%S S-edge. However, the 50%S S-edge is found to be mildly unstable with respect to H_2S in the presence of water/OH. Hence, we suggest that the 50%S S-edge evolves over time towards a 0%S S-edge, covered by surface OH that will block permanently the active sites.

Introduction

In recent years, transition metal disulfides (TMDs) have attracted much attention due to their abundance, low cost, and catalytic activity.[1–5] Because of its natural occurrence, and potential use in numerous applications (from catalysis to solid lubricants),[6] the most studied

material in the TMD series is molybdenum disulfide, MoS_2.[7,8] Since it is a 2D material, MoS_2 particles have a basal plane and edges with contrasting chemical properties. There is a general consensus that the edges of the most common 2H-MoS_2 polymorph are the catalytically active sites, while the defect-free basal plane is inert.[9]

There are different types of edges in MoS_2 with various properties.[10–12] As represented in Figure 1, two families of edges can be distinguished for 2H-MoS_2: the armchair edges $(\bar{1}2\bar{1}0)$ and the zigzag edges, for which the Mo-edge $(\bar{1}010)$ and S-edge $(10\bar{1}0)$ have distinct chemical properties.[13] Theoretical[14] studies show that zigzag edges are much more stable than armchairs, so that experimentally only the zigzag edges have been identified.[15,16]

Many studies have approached the problem of the edge configuration and their relative stability. Most of these studies have been carried out in the context of the hydrodesulfurization (HDS) reaction, for which MoS_2 is a typical catalyst.[17,18] HDS removes sulfur from natural gas and from petroleum to reduce polluting emissions upon combustion. Under HDS conditions MoS_2 is exposed to a mixture of H_2 and H_2S gases. Therefore, the relative stability of edges with different sulfidation levels is governed by the relative abundance of H_2 and H_2S. The first density functional theory (DFT) based thermodynamic model was developed by Raybaud et al.[19] for the zigzag edge. This theoretical study suggested that the 100%S S-edge and the 50%S Mo-edge are the most stable sulfidation levels under typical, S-rich, HDS conditions. The 50%S Mo-edge is particularly stable due to the reconstruction of the structure that satisfies the coordination needs of Mo and S atoms. Hence, transformation to more or less sulfided Mo-edges is suggested to be an activated process.[20] For the stoichiometric case, i.e., absence of excess S, the most stable distribution of S over the Mo and S edge was predicted to be semi-saturated (50%S) on both edges. This also corresponds to typical sulfur poor conditions.[19,21]

Complementary to the computational work, various experimental studies have been carried out to determine the structure, activity and stability of MoS_2 edges, mostly relying on scanning tunneling microscopy (STM).[20,22–26] Despite a general agreement between the-

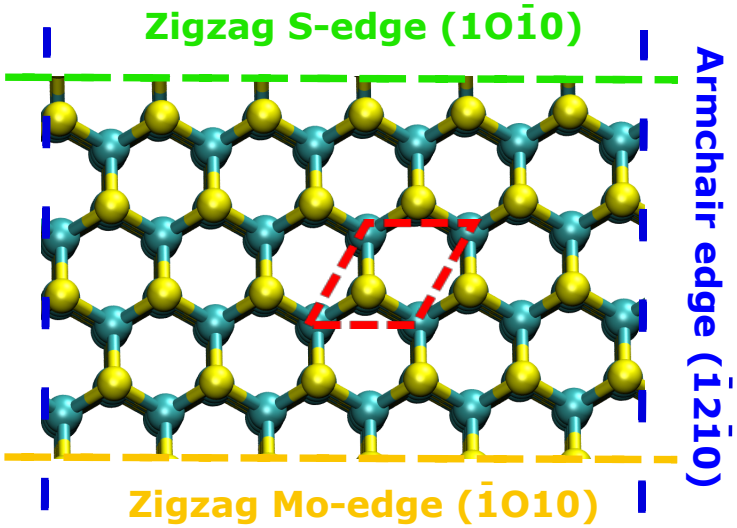

(a) Different types of MoS_2 edges

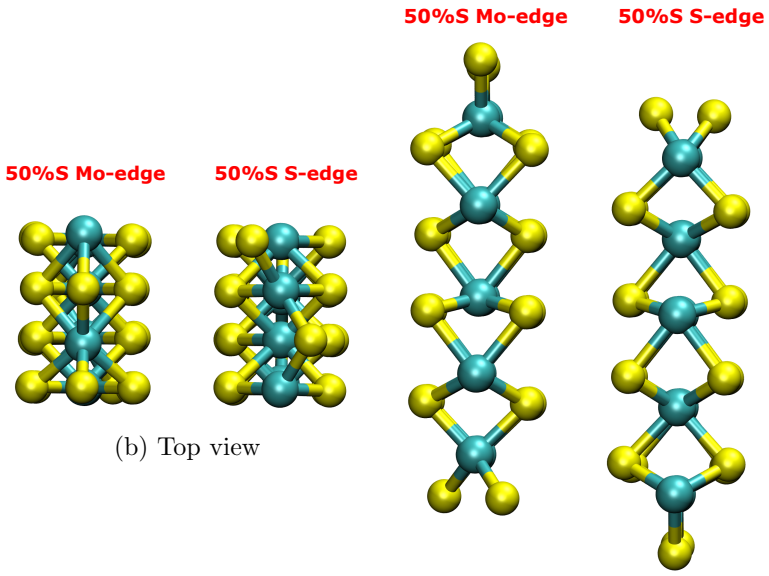

(b) Top view

(c) Side view

Figure 1: (a) Classification of MoS_2 edges according to the way a single layer of 1H-MoS_2 is truncated. The crystallographic indices and common names of these edges are given. Two types of edges are shown: Zigzag and armchair edges. Because of the symmetry of MoS_2, there are two types of zigzag edges: Mo-edge and S-edge, (b) Top and (c) Side views of 50%S S-edge and 50%S Mo-edge. The color code for atoms is yellow for S and greenish for Mo.

ory and experiment, the prevalent structure of the active sites during hydrodesulfurization catalysis on MoS_2 is still debated.[27]

The interest in MoS_2 based electrocatalysts started in 2005, when Hinnemann et al.[28] demonstrated, through computational and experimental methods, that MoS_2 is a promising low-cost electrocatalyst for hydrogen evolution reaction (HER). HER, the half-cell reaction of water splitting, is typically investigated for applications at ambient temperature, in an acidic, aqueous electrolytes. Therefore, the reaction conditions are very different from high-temperature, gas-phase HDS. Inspired by this seminal work,[28] several groups have explored the electrocatalytic activity of molybdenum disulfide and how to improve it.[29,30] Jaramillo et al.[31] synthesized MoS_2 on Au(111) substrate and showed that the HER activity of MoS_2 increases linearly with the total length of the exposed edges of MoS_2. Tan et al.[32] also presented that the edge site showed much higher activity for HER than the basal plane. Since then, numerous experimental studies have reported that although the edge occupies a small portion of the surface area of MoS_2, the HER active site is mainly located at the zigzag edges and only a minority of active sites are located on the basal plane.[1,33–36]

For theoretical identification of active sites, the adsorption energy of hydrogen, ΔG_H, is typically used as a descriptor.[37,38] A positive ΔG_H value indicates that the interaction between H and the catalyst is too weak for efficient catalysis. A negative value indicates that the interaction is too strong, i.e., desorbing gaseous H_2 is energetically too costly. The adsorption of hydrogen on the edge of 2H-MoS_2 strongly depends on the edge type and the sulfidation level.[33,34,39,40] The most favorable hydrogen bonding with respect to HER was found for the edge covered by sulfur monomers (50%S Mo-edge). This edge is stable under a wide range of sulfidation conditions and should therefore be abundant in the catalytic particles. Furthermore, the 50%S Mo-edge and the 50%S S-edge configurations are the most representative ones obtained by the large-scale preparation of MoS_2 catalysts via wet-impregnation followed by sulfidation. For all hydrogen coverages between $\theta_H = 0\%$ and $\theta_H = 100\%$, the adsorption energy of hydrogen at 50%S Mo-edge is about 0 eV.[41]

Therefore, this surface state was, for instance, used by Goddard and coworkers for a detailed mechanistic study of HER.[42] Note, however, that assessing the stability of the S-coverage at the edges under HER conditions is somewhat ill-defined: while there is a constant source of sulfur under HDS conditions, in HER only the chemical potential of hydrogen is well defined. Hence, loss of sulfur atoms in form of H_2S under these acidic reducing conditions is irreversible, an aspect that has been largely neglected in the HER literature.

Since HER takes place in liquid water at ambient temperature, one should also evaluate the reactivity and stability of MoS_2 edges towards H_2O. However, only few, theoretical, studies have been devoted to the interaction between water and the MoS_2 edges. Singh et al.,[43] studied water dissociation, including the corresponding activation energies, over the three thermodynamically stable edges reported by Raybaud et al. (0%S Mo-edge, 50%S S-edge, and 100%S S-edge).[19] The process was found to be exothermic only for both 50%S S-edge and 0%S Mo-edge, with the 0%S Mo-edge having the lowest activation energy barrier. Ab initio molecular dynamics (AIMD) further confirmed a spontaneous dissociation of water on the 0%S Mo-edge, demonstrating that this surface termination is unstable and thus irrelevant in aqueous solution. The impact of the reactivity of the edges towards water has been considered as part of our previous study[44] that focused on HER over MoS_2 explicitly accounting for the electrochemical potential via grand-canonical DFT in combination with the linearized Poisson-Boltzmann equation.[45,46] Contrary to current proposals, many of the identified active sites involve adsorbed OH*. In other words, we have shown that although H_2O and OH can adsorb on MoS_2, HER can also occur on these "blocked" active sites by reducing protons on surface OH*/H_2O entities.

Here, we investigate the stability of the MoS_2 edges and the impact on HER of the changes due to reactions with water. The adsorption of H, H_2O and electrochemically generated OH* is studied in detail on these edges. Then, we assess the possibility for H_2S release from these edges. Finally, relying on grand-canonical DFT we demonstrate the possibility of HER even on the desulfided edges via OH/H_2O cycles.

Methods

Computational details

The first-principles calculations are performed using the periodic DFT code "Vienna ab initio simulation package", VASP.[47] We have adopted the generalized gradient approximation density functional PBE-dDsC,[48,49] which is augmented with a density-dependent dispersion correction.[50] The nuclei and core electrons are described by the projector augmented wave function approach (PAW).[51,52] A plane-wave basis set with a kinetic energy cutoff of 500 eV is used for the valence electrons. The precision setting of VASP is set to "accurate". We used a Fermi smearing corresponding to room temperature (0.025 eV) and a Monkhorst-Pack $3 \times 3 \times 1$ k-point mesh for all the studied surfaces p(2×1), p(3×1) and p(4×1). The convergence criterion for the self-consistency process is set to 10^{-5} eV for the optimization of the wave function. The maximum forces are converged to below 0.025 eV/Å during the geometry optimization. All edges are five layers thick, leading to well converged adsorption energies. Above and below the slabs, approximately 15 Å of vacuum is added in the z-direction.[53] The electrochemical interface, where HER occurs, is described by electronic DFT for the electrode and adsorbates, combined with a continuum solvation model, augmented with an implicit electrolyte, both represented by the solution of the linearized Poisson-Boltzmann equation as implemented in VASPsol.[45] As in our previous study,[44] the "critical" density, ρ_c which defines the interface is set to 0.00025 $e^-/\text{Å}^{-1}$, which is equivalent to one-tenth of the default value in order to prohibit the implicit solvent from entering between the MoS_2 layers. This makes the DFT computations slower than usual due to the associated larger numerical noise, but has also been used previously in the context of solvated alkali-metal ions.[54,55] The Debey screening length is set to 3 Å, which corresponds to a 1 M electrolyte. This is representative for 0.5 M aqueous H_2SO_4 solutions typically used in HER experiments. To properly define the work-function (electrochemical potential) of the interface, the dipole moment of the slab needs to be nullified through symmetry. We perform

a point symmetrization for all the edges. The central layers are kept frozen in their bulk positions. The potential dependence is studied by varying the number of electrons.[53,56] In practice, the charge of the system is varied from -1 to +1 in steps of 0.2 e^- (see example and script provided in the SI). The non-integer system charges are neutralized via the Poisson-Boltzmann equation, similar to other grand canonical DFT schemes in the literature.[57–64] The obtained relation between the grand-canonical energy and the electrochemical potential is then fitted to an analytical formula, which is a parabola for conductors. This approach was previously applied for the elucidation of reaction mechanisms at electrified interfaces such as the oxygen evolution reaction[65,66] and for elucidating the origin of the electrochemical promotion of catalysis.[56,67]

Reaction energies

For isolated molecules we use the following approximation for their free energy:

$$G_{mol} = E_{mol} - TS \tag{1}$$

where T is room temperature (298.15 K), and S is the contribution of rotational translational entropy at standard pressure. For water, this entropy contribution is divided by two to account for its liquid state.[68,69]

If not stated otherwise, the adsorption energy, ΔG_{ads}, of the different species are calculated in the framework of the computational hydrogen electrode (CHE)[70] at 0 V and pH 0, representative for acidic HER:

$$G_{ads} = \frac{1}{2} \times (E_{tot} - E_{slab} - R) \tag{2}$$

Where E_{tot} and E_{slab} are the energies of the symmetric MoS_2 surface with and without adsorbates, respectively. When the adsorbate is hydrogen (i.e., one hydrogen atom per surface), the energy of the reactant is defined as R = $G_{H_2(g)}$, where $G_{H_2(g)}$ is the free energy

of the hydrogen molecule. For the adsorption of the water molecule, R = $2G_{H_2O}$. For OH adsorption under the relevant reducing conditions, we set $R = G_{H_2(g)} - 2G_{H_2O}$. In other words, OH* is formed by adsorption of H_2O with a subsequent electroreduction (formally a Heyrovsky step) that releases H_2.[44]

Similarly, we assess the stability of the edges with respect to the release of H_2S:

$$\Delta G_{release_1} = \frac{1}{2} \times (E_{decomp} + 2G_{H_2S} - E_{tot}) \tag{3}$$

Where E_{tot} and E_{decomp} are the energies of the symmetric MoS_2 surface with H_2S (in the form of at least 50% H coverage on the 50%S edges) and the "decomposed" edge, i.e., after loss of H_2S, respectively. G_{H_2S} is the free energy of the H_2S molecule. If $G_{release_1}$ is equal to 0 eV, it is an isothermal process. A negative value indicates that the reaction is spontaneous. A positive value indicates that the process is not spontaneous under standard conditions. Note, however, that under HER conditions the partial pressure of H_2S is essentially very small (a low range of 10^{-5} to 10^{-8}),[34] so that even endergonic reactions have a finite probability to occur. Note that the loss of sulfur under acidic HER conditions most likely occurs as H_2S.

An alternative of this "decomposition" reaction is the "substitution" reaction: H_2S can be released in combination with water adsorption. The formula of the release energy is:

$$\Delta G_{release_2} = \frac{1}{2} \times (E_{subst} + 2G_{H_2S} - E_{tot} - 2G_{H_2O}) \tag{4}$$

Where E_{tot} and E_{subst} are the energies of the (initial) symmetric MoS_2 surface with hydrogen bonding to sulfur and the (substituted) edges with hydrogen bonded to oxygen, respectively. G_{H_2S} and G_{H_2O} are the free energies of the H_2S and H_2O molecules. The criterion for determining the thermodynamic nature of the process is the same as for Eq.3.

Hydrogen production by H_2O, OH and O cycling

Our earlier study showed that adsorbed OH* and H_2O species can participate in HER. This OH* differs from the adsorption of OH^-, as it is associated with water reduction and should be considered as an adsorbed hydroxyl "radical" and thus accessible in acidic, reducing conditions. Similarly, we here investigate the stability and activity of such active sites on the 50%S S-edge; 50%S Mo-edge. The corresponding catalytic cycle is schematically depicted on Figure 2. Adsorbate A_1, which is also a reaction intermediate, can be O or OH, while the corresponding intermediate A_2 is OH or H_2O, respectively. In these catalytic cycles, the reactions connecting the intermediates are the addition of a $H^+ + e^-$ pair, with ΔG_1 resembling a Volmer and ΔG_2 a Heyrovsky step, respectively. Fore these catalytic cycles, we perform grand-canonical DFT computations in order to explicitly study the potential dependence. In practice, the charge of the system is varied from -1 to $+1$ with a step length of 0.2 e^- and it is neutralized via the Poisson-Boltzmann equation in close analogy with our previous works.[44,65] The acquired connection between the grand-canonical energy and the electrochemical potential is then fitted to an analytical formula, which is a parabola for conductors.

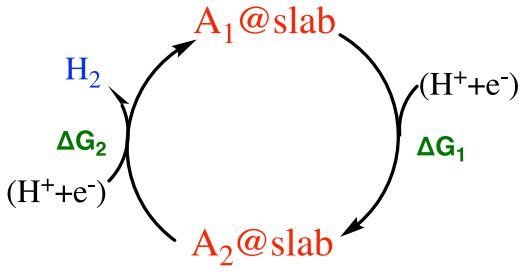

Figure 2: H_2 evolution via cycling between OH and H_2O or O and OH. ΔG_1 corresponds to a Volmer step (adsorption of $H^+ + e-$), while ΔG_2 is a Heyrovsky step.

Hydrogen production by these cycles can only occur when the ΔGs are less than or near zero. They are calculated as a function of the electrochemical potential according to the

following formulas:

$$\Delta G_1(U) = \frac{1}{2} \times (E_{tot}(A_2)(U) - E_{tot}(A_1)(U) - 2 \times (\mathrm{H^+ + e^-})) \quad (5)$$

$$\Delta G_2(U) = \frac{1}{2} \times (E_{tot}(A_1)(U) + 2 \times G_{\mathrm{H_2}} - E_{tot}(A_2)(U) - 2 \times (\mathrm{H^+ + e^-})) \quad (6)$$

Where $E_{tot}(A_1)(U)$ and $E_{tot}(A_2)(U)$ are the potential dependent energies of the symmetric MoS_2 edges with O or OH for A_1 and with OH or H_2O for A_2. $G_{\mathrm{H_2}}$ is the free energy of the hydrogen molecule, and U is the applied potential with respect to the standard hydrogen electrode.

As pointed out by Norskov and coworkers, the chemical potential of protons and electrons can be conveniently replaced by that of hydrogen molecules and the energy correction for the electron due to the electrode potential.[70] Therefore, $2 \times (H^+ + e^-) = 2\mu_H(U) = G_{\mathrm{H_{2(g)}}} - 2eU$ at pH=0, as we evaluate here HER under acidic conditions.

Results and discussions

Hydrogen adsorption

While under HDS conditions there is a constant source of sulfur and thus the sulfided edges are stable, in HER only the chemical potential of hydrogen is well defined. Hence, the loss of sulfur atoms in the form of H_2S is irreversible for HER. Therefore, the most stable, reconstructed, 50%S S-edge in combination with 50%S Mo-edge (see Figure S1 and Figure 3), which is the most stable stoichiometric edge, is the common starting point for HER investigations.[42] Herein, we start by revisiting the expected hydrogen coverage of these edges under the hydrogen evolution reaction conditions, i.e., including the continuum solvent and a potential of 0 V vs SHE, the thermodynamic onset potential at pH 0. The first step was to locate promising hydrogen adsorption sites (see Figure S2). ΔG_H is very close to 0 eV in all cases. The most stable adsorption site is on the "side" of the 50%S S-

edge, with an adsorption energies of 0.04 eV. For the second hydrogen adsorption, the most promising sites are the "side" site (-0.01 eV). The top S site is somewhat peculiar: the first hydrogen adsorption energy is endergonic (0.38 eV), while the second one is exergonic (-0.14 eV). Given that the average remains less favorable than the "side" adsorption mode, these top-modes are likely to be relevant only at high H coverages. Based on these results, we investigated the overall hydrogen adsorption as a function of the H coverage for the MoS_2 50 %S edges. Assessing various combinations, we identified the most stable step-wise H adsorption sequence: hydrogen 1 to 6 as shown in Figure 3. With increasing θ_H, the ΔG_H becomes weaker which is in complete agreement with the previously reported results of MoS_2[71] and with other transition metal dichalcogenides and phosphides in general.[72,73] ΔG_H of the first to the fourth hydrogen is very close to 0 eV (from -0.17 eV to 0.33 eV). This opens the possibility for H_2 release via the Volmer-Tafel mechanism under the condition that the activation energy for the (chemical) Tafel step is not too high.

H_2O/OH adsorption and H co-adsorption

We now move to the adsorption of the solvent (H_2O) and OH which can be generated under HER conditions on the MoS_2 edges.[44]

As illustrated in Figure 4, H_2O adsorption is nearly thermoneutral for both the 50%S S-edge and the 50%S Mo-edge. For the 50%S S-edge, where H_2O is more strongly adsorbed, the oxygen atom is in the "side" position and one hydrogen atom points away from the surface, while the other lies in the surface plane, pointing toward the neighboring MoS_2 layer. At the 50%S Mo-edge, the water molecules are just physisorbed, with one hydrogen atom pointing towards the sulfur surface atom, establishing the closest contact between water and the surface. For both edges, the OH bond lengths in the adsorbed water molecule are slightly larger (0.978 Å) than those of a free H_2O molecule (0.958 Å), indicating that the OH bond is slightly weakened when the molecule is in contact with the MoS_2 edge.

In contrast to H_2O, OH is only adsorbed at the 50%S S-edge, especially when there is

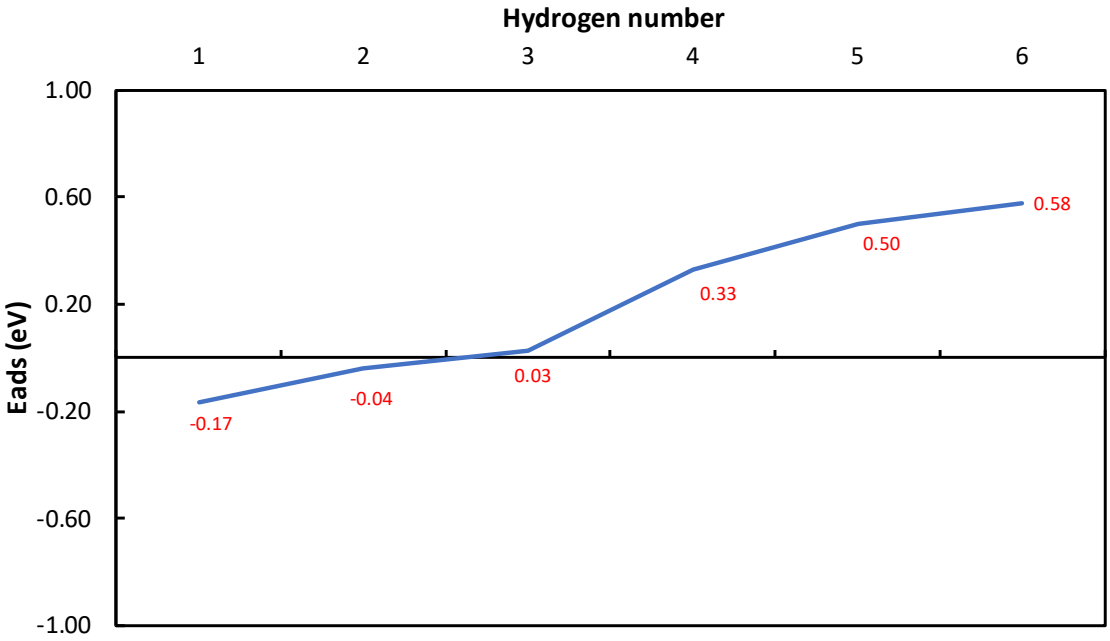

(a) The Hydrogen adsorption energies as a function of the Hydrogen coverage.

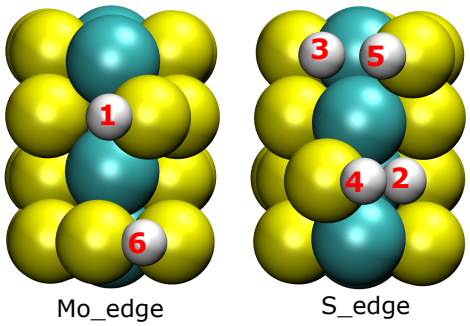

(b) Visualization of the MoS_2 edges with the different hydrogen adsorbed.

Figure 3: Hydrogen adsorption on 50%S S-edge and 50%S Mo-edge .The color code for atoms is white for H; yellow for S and greenish for Mo.

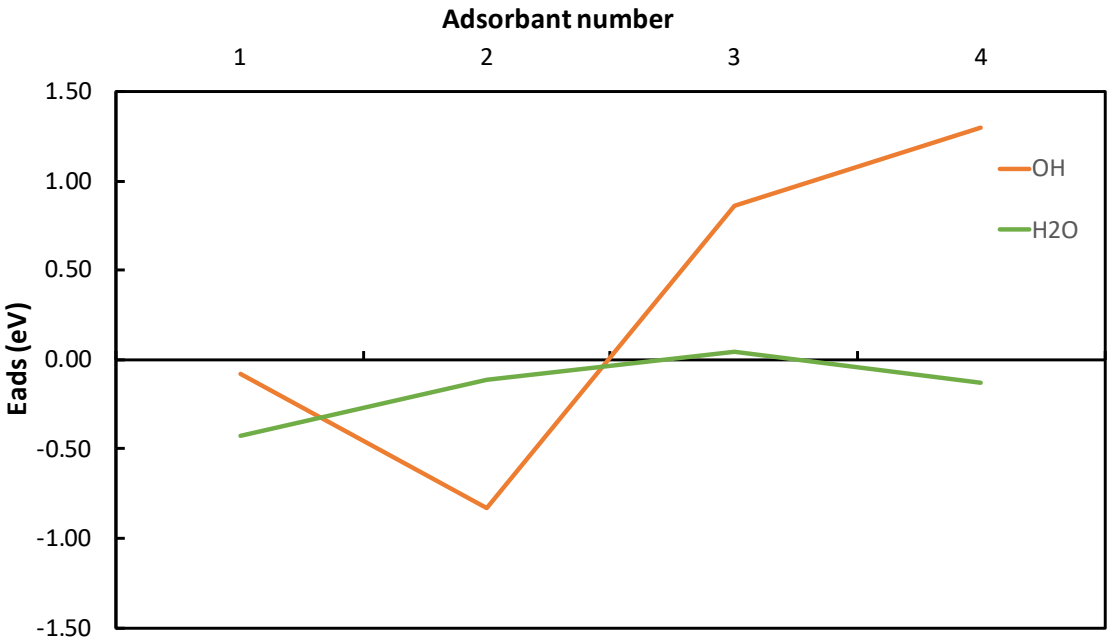

(a) adsorption energies of OH and H_2O on the different edge sites.

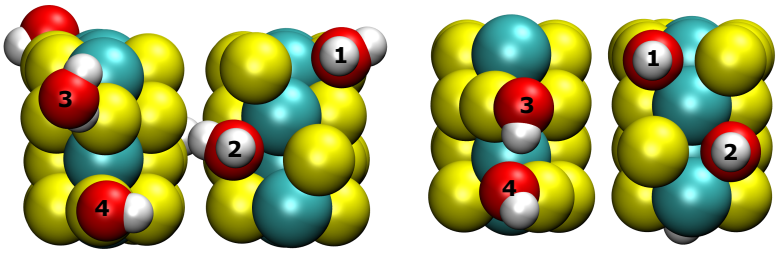

(b) H_2O (c) OH

Figure 4: The adsorption energies of OH and H_2O on MoS_2 edges with visualisation of the structures. The color code for atoms is white for H; red for O; yellow for S and greenish for Mo.

one $\theta_{OH} = 1$. The OH adsorption energy on the 50%S Mo-edge is, however, above 1 eV. This difference is explained by the accessibility of the Mo atom in the "side" adsorption mode on the 50%S S-edge, while the Mo atoms of the 50%S Mo-edge are completely inaccessible.

These results reveal that there is a competition between H and OH at the 50%S S-edge, while H_2O seems to be rather labile over both edges.

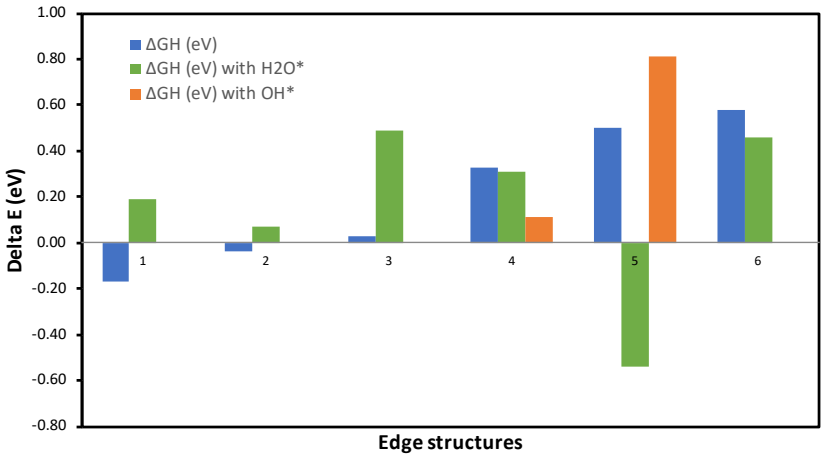

Figure 5: Comparison of the different ΔG_H values without and with the presence of OH and H_2O. The numbering of the H atoms is the same as in Fig. 3

In view of the competition of H and OH and knowing that H_2O will be present anyway, we assess ΔG_H in the presence of OH and H_2O. The different combinations tested are reported on Figure S3, while Figure 5 summarizes ΔG_H for the various cases. Note that our tests show that the adsorption energy of one species is not affected by the presence of another molecule at the "other" edge, i.e., the Mo-edge and S-edge can be considered "decoupled" (see Figure S4).

For the 50%S Mo-edge, we observe that the presence of H_2O does not qualitatively change the conclusion: The first hydrogen atom (number 1 in Fig. 5 is weakly adsorbed (the sign changes in presence/absence of water, but the adsorption energy remains weak), while the second one (number 6) features a clearly positive adsorption energy. For the 50%S S-edge, hydrogen number 2 and 4 are not affected by H_2O, i.e., green and blue bars are close to each other. This is not the case for hydrogen 3, for which ΔG_H reaches 0.49 eV in presence of H_2O,

while it was thermoneutral in the absence of the water molecule. Hydrogen 5 "compensates" this endothermicity, i.e. it is very strongly adsorbed in the presence of water, while it was costly in the absence of co-adsorption (-0.54 eV and 0.5 eV, respectively). The case of OH co-adsorption is restricted to hydrogen 4 and 5: The OH take the place of hydrogen 2 and 3. The effect of OH on hydrogen 4 is only ~ 0.2 eV, making H adsorption nearly thermoneutral. However, adsorbing a second hydrogen atom (number 5) becomes prohibitive $\Delta G_H = 0.8$ eV.

In summary, water modulates the hydrogen adsorption energy, but, in agreement with the weak adsorption energy of water on these edges, the overall H coverage is only marginally affected by the solvent. In contrast, the presence of OH groups on the "side" positions of the 50%S S-edge, where they are easily formed (see Fig. 4), reduces the H coverage on the S-edge significantly.

Edge Stability

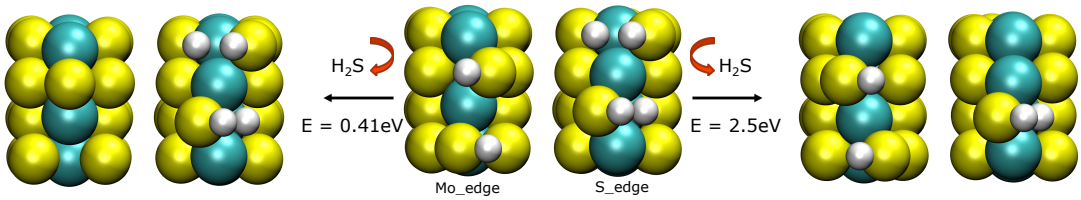

Figure 6: H_2S release on 50% S Mo-edge and 50% S S-edge after H adsorption. The color code for atoms is white for H; yellow for S and greenish for Mo.

An important aspect of MoS_2 electrocatalysts is their (long-term) stability. In contrast to HDS applications, there is no sulfur reservoir under HER conditions. Hence, we here estimate the thermodynamic stability of the edges. As shown in two preceding sections, the hydrogen coverage is significant ($\sim$ 1 monolayer (ML) with respect to the Mo edge atoms) under HER conditions. Therefore, we start by computing the reaction energy for H_2S release (see Figure 6), a typical process known in the literature in the context of hydrogen rich HDS conditions. At the 50%S S-edge, we find that the process is very endothermic (2.5 eV). In contrast, the

50%S Mo-edge is significantly less stable and H_2S desorption is endergonic by only 0.41 eV. Note that this reaction energy assumes standard conditions (1 bar of H_2S). Hence, under HER conditions (no partial pressure of H_2S), the loss of H_2S is certainly facilitated compared to this estimate. Furthermore, in the absence of a S reservoir, any sulfur that is lost from the surface has no chance to be replenished. Hence, we conclude that the sulfur coverage of the 50%S Mo-edge will decrease over time until it reaches the 0%S Mo-edge. Fortunately for HER, this edge is expected to be reasonably active as well,[44] so that activity should not drop significantly over time despite the structural rearrangements. As for the 50%S S-edge, it seems to be stable in the presence of H, i.e., the adsorbed hydrogen atoms can participate in the HER mechanism.

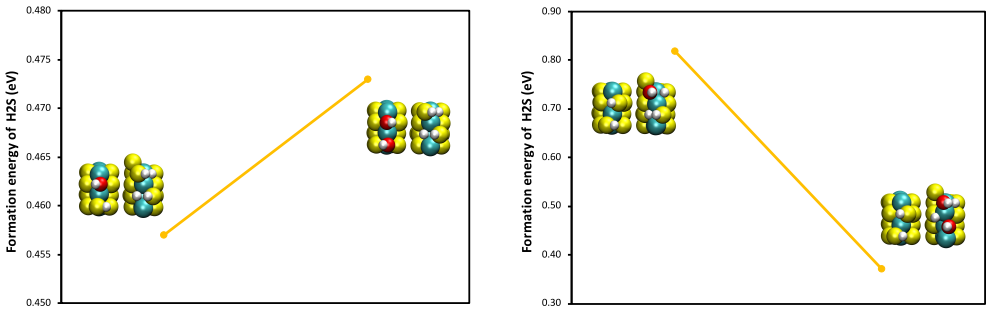

(a) H_2S release on 50%S Mo-edge (b) H_2S release on 50%S S-edge

Figure 7: H_2S release on 50%S Mo-edge and 50%S S-edge after OH adsorption. The color code for atoms is white for H; red for O; yellow for S and greenish for Mo.

The above estimates have been performed without the consideration of the actual reaction medium which is an aqueous solution. As discussed above, OH can be generated in situ under HER conditions. Hence, we here investigate an "exchange" reaction, where the edge sulfur atoms are replaced by oxygen. To be precise, we assess the following reaction: $E{-}SH + H_2O \longrightarrow E{-}OH + H_2S$, where "E" symbolizes the remaining atoms of the edge. Figure 7 shows that for the Mo-edge it is possible to release H_2S with nearly the same exchange reaction energy for the first OH as for the second OH (0.4-0.5 eV). Furthermore, this energy is very similar to the loss of H_2S of Fig. 6. For the S-edge, the exchange reaction energy is

significantly more energy consuming for the first OH (0.8 eV) than for the Mo-edge, although still much lower than the H_2S desorption energy. However, replacing the second OH by SH is as feasible as on the Mo edge.

These results indicate that the stability of the 50%S Mo-edge is rather limited under HER condition, which H_2S desorption, potentially assisted by H_2O/OH adsorption being rather likely. The 50% S-edge is somewhat more stable. Nevertheless, in the absence of estimates concerning the reaction barrier for the E−SH $\longrightarrow$ E−OH exchange reaction under HER conditions, it is difficult to judge how much this decomposition reaction contributes to the long-term (in-)stability of the MoS_2 electrocatalyst. It must be noted that the 0%S Mo-edge is likely to remain active for HER.[44] This is, however, not the case for the 0%S S-edge: According to our computations (see Fig. S5), this edge termination is permanently blocked by OH, rendering this edge inactive for HER.

HER mechanism over 50%S S-edge in presence of water

As shown above, the MoS_2 edges react with the water solvent under HER conditions. Hence, we here revisit the HER reaction mechanism starting with the most relevant surface state. In particular, the 50%S S-edge is likely to be partially covered by OH. For the Mo-edge, the adsorbed water molecules are very unlikely to dissociate, since OH is poorly adsorbed (see OH 3 and 4 of Fig. 4). To assess the possibility of hydrogen production, we assessed different catalytic cycles. For the S-edge, Figure 8 shows the most relevant energy profile at 0 V. We start with the edge structure on which four water molecules are physisorbed, two spectators at the Mo-edge and the other two at the S-edge. At this potential, the Heyrovsky reaction releasing H_2 and concomitantly forming OH on the S-edge is exothermic. At this stage there are three pathways, two of which are endothermic, so we continue with the exothermic one, which leads to two OH adsorbed on the S edge. This surface state still presents three possible paths that could lead to HER: A Heyrovsky step with an OH hydrogen, a Volmer step on an OH, or a Volmer step on an S site. Our grand-canonical DFT computations demonstrate

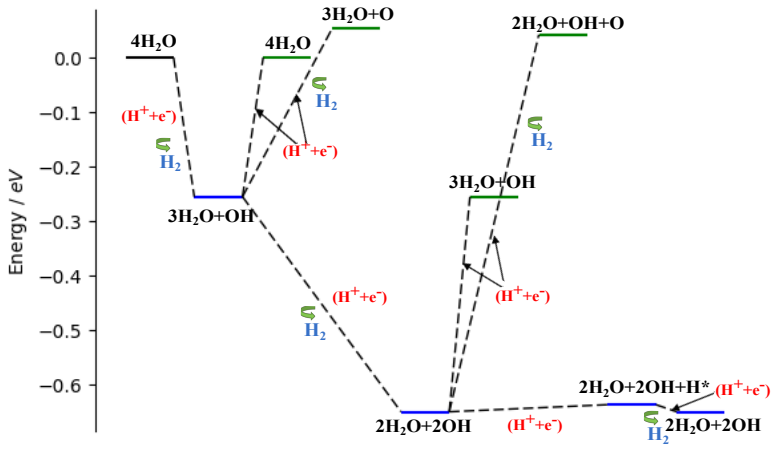

(a) Reaction energy profile at 0 V

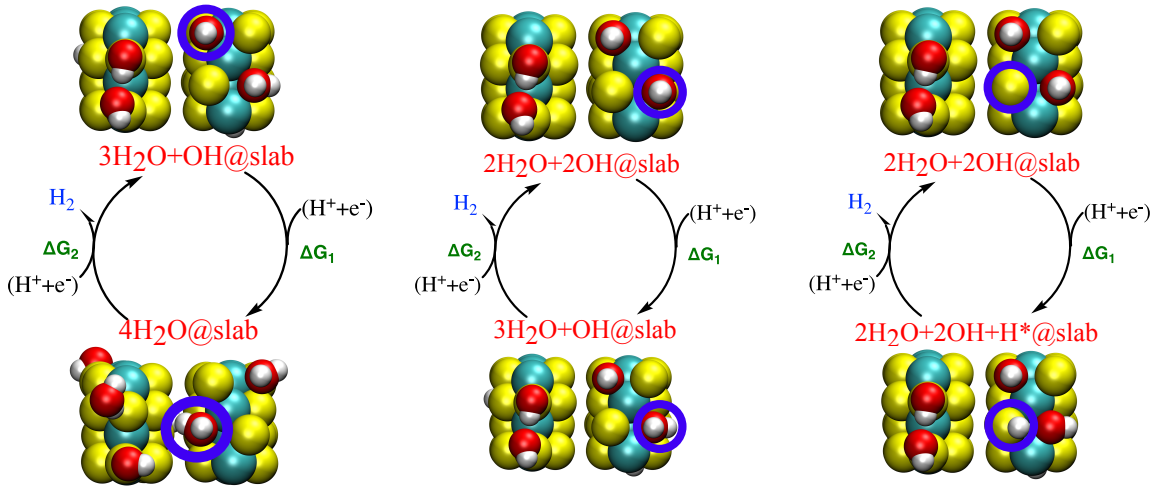

(b) first cycle (c) second cycle (d) Third cycle

Figure 8: (a) Production of H_2 on the water covered S-edge, involving H_2O, OH and H*. The thermodynamic over-potential η_{TD} is determined to be 0 V. The possible steps are designed by the blue color whereas the green color is for the blocking steps. (b) The first cycle with $\Delta G_1 = 0.225$ eV and $\Delta G_2 = -0.225$ eV. (c) The second cycle with $\Delta G_1 = 0.394$ eV and $\Delta G_2 = -0.394$ eV. (d) The third cycle with $\Delta G_1 = 0.014$ eV and $\Delta G_2 = -0.014$ eV. The color code for atoms is white for H; red for O; yellow for S and greenish for Mo. The circle blue indicates the site where the different steps occur.

that only the latter is energetically feasible, leading to S-H. Several reactions could proceed with this S-H (see Fig. S6): (i) in combination with an additional proton reduction H_2S could be released, (ii) an SH*/OH* exchange reaction or (iii) H_2 production via a Heyrovsky step. The first of these reactions one is strongly endothermic. The second one is mildly endothermic (0.2 eV) and thus likely to be feasible but slow under HER conditions. However, once this reaction occurs and we reach an edge covered by 3 OH*, on which the Volmer step is endergonic by 0.4 eV, so that the HER activity is lost. The last possibility is the HER reaction, which turns out to b athermic as indicated in Fig. 8d.

Therefore, we demonstrate that despite the presence of two surface OH entities on the 50%S S-edge, the sulfur sites could remain catalytically active via a Volmer Heyrovsky mechanism at near zero overpotential.

Conclusion

We have analyzed the fate of the most commonly produced MoS_2 edge, i.e., the 50%S S-edge; 50%S Mo-edge, under HER conditions. While this Mo-edge could potentially be active for HER with an estimated overpotential of about 0.2 V, we reveal that this edge is very likely to significantly reconstruct in the presence of water. In particular, H_2S formation is only mildly endothermic ($\sim$0.4 eV), so that under HER conditions, where there is no sulfur reservoir, surface-sulfur is gradually replaced by oxygen. Fortunately, the thus formed surface OH are active sites for HER. The situation on the 50%S-edge is less straight forward. First, the termination is more stable with respect to H_2S release (ΔG = 2.5 eV). Second, though, the exchange reaction that replaces surface SH by surface OH is endothermic by only 0.8 eV. Once the first such exchange reactions has occurred, the second one is facilitated. Furthermore, this OH substituted S-edge is no longer predicted to be active for HER. Hence, this exchange reaction appears to lead to a definite loss of HER activity of MoS_2. Third, our grand-canonical DFT computations suggest that before the loss of surface sulfur, the

S atoms of this edge are active sites for HER even in the presence of surface OH, with an estimated overpotential of 0 V.

In summary, our findings provide an atomistic description of the fate of the common 50%S S-edge, 50%S Mo-edge edge structure of MoS_2 under HER conditions. The likely active sites in presence of water have been identified and their stability has been assessed, revealing long-term stability issues of the S-edge in water, a prediction that could be experimentally verified by operando X-ray spectroscopies.

Acknowledgement

This work was financially supported by Région Auvergne Rhône-Alpes through the project Pack Ambition Recherche 2018 MoSHi. We are very grateful to IFP Energies nouvelles for supporting the MoSHy project (N^o 1801167601) and to the IFP Energies nouvelles team, Mona Marie Obadia and Quentin Cacciuttolo, for fruitful discussions. The authors thank the SYSPROD project and AXELERA Pôle de Compétitivité for financial support (PSMN Data Center).

Supporting Information Available

The supplementary material contains the discussion of the stability of the 50%S reconstructions of the MoS_2 edge, additional Figures and Tables. Coordinates and DFT raw data is freely available on NOMAD-lab: `https://dx.doi.org/10.17172/NOMAD/2021.05.18-1` The script to post-process VASP computations to GC-DFT is provided.

References

(1) Laursen, A. B.; Kegnæs, S.; Dahl, S.; Chorkendorff, I. Molybdenum sulfides—efficient and viable materials for electro-and photoelectrocatalytic hydrogen evolution. *Energy*

Environ. Sci. **2012**, *5*, 5577–5591.

(2) Wang, H.; Lu, Z.; Xu, S.; Kong, D.; Cha, J. J.; Zheng, G.; Hsu, P.-C.; Yan, K.; Bradshaw, D.; Prinz, F. B., et al. Electrochemical tuning of vertically aligned MoS2 nanofilms and its application in improving hydrogen evolution reaction. *Proc. Natl. Acad. Sci. U.S.A.* **2013**, *110*, 19701–19706.

(3) Voiry, D.; Yamaguchi, H.; Li, J.; Silva, R.; Alves, D. C. B.; Fujita, T.; Chen, M.; Asefa, T.; Shenoy, V. B.; Eda, G., et al. Enhanced catalytic activity in strained chemically exfoliated WS 2 nanosheets for hydrogen evolution. *Nat. Mater.* **2013**, *12*, 850–855.

(4) Tan, C.; Zhang, H. Two-dimensional transition metal dichalcogenide nanosheet-based composites. *Chem. Soc. Rev.* **2015**, *44*, 2713–2731.

(5) Karunadasa, H. I.; Montalvo, E.; Sun, Y.; Majda, M.; Long, J. R.; Chang, C. J. A molecular MoS2 edge site mimic for catalytic hydrogen generation. *Science* **2012**, *335*, 698–702.

(6) Chhowalla, M.; Shin, H. S.; Eda, G.; Li, L.-J.; Loh, K. P.; Zhang, H. The chemistry of two-dimensional layered transition metal dichalcogenide nanosheets. *Nat. Chem.* **2013**, *5*, 263–275.

(7) Song, I.; Park, C.; Choi, H. C. Synthesis and properties of molybdenum disulphide: from bulk to atomic layers. *RSC Adv.* **2015**, *5*, 7495–7514.

(8) Ganatra, R.; Zhang, Q. Few-layer MoS2: a promising layered semiconductor. *ACS nano* **2014**, *8*, 4074–4099.

(9) Lei, B.; Li, G. R.; Gao, X. P. Morphology dependence of molybdenum disulfide transparent counter electrode in dye-sensitized solar cells. *J. Mater. Chem.A* **2014**, *2*, 3919–3925.

(10) Schweiger, H.; Raybaud, P.; Kresse, G.; Toulhoat, H. Shape and edge sites modifications of MoS2 catalytic nanoparticles induced by working conditions: a theoretical study. *J. Catal.* **2002**, *207*, 76–87.

(11) Füchtbauer, H. G.; Tuxen, A. K.; Li, Z.; Topsøe, H.; Lauritsen, J. V.; Besenbacher, F. Morphology and atomic-scale structure of MoS 2 nanoclusters synthesized with different sulfiding agents. *Top. Catal.* **2014**, *57*, 207–214.

(12) Liu, Y.; Wang, H.; Yuan, X.; Wu, Y.; Wang, H.; Tan, Y. Z.; Chew, J. W. Roles of sulfur-edge sites, metal-edge sites, terrace sites, and defects in metal sulfides for photocatalysis. *Chem. Catal.* **2021**,

(13) Yu, S.; Zheng, W. Fundamental insights into the electronic structure of zigzag MoS 2 nanoribbons. *Phys. Chem. Chem. Phys.* **2016**, *18*, 4675–4683.

(14) Cao, D.; Shen, T.; Liang, P.; Chen, X.; Shu, H. Role of chemical potential in flake shape and edge properties of monolayer MoS2. *J. Phys. Chem. C* **2015**, *119*, 4294–4301.

(15) Wang, Z.; Li, H.; Liu, Z.; Shi, Z.; Lu, J.; Suenaga, K.; Joung, S.-K.; Okazaki, T.; Gu, Z.; Zhou, J., et al. Mixed low-dimensional nanomaterial: 2D ultranarrow MoS2 inorganic nanoribbons encapsulated in quasi-1D carbon nanotubes. *J. Am. Chem. Soc.* **2010**, *132*, 13840–13847.

(16) Xu, H.; Ding, Z.; Nai, C. T.; Bao, Y.; Cheng, F.; Tan, S. J. R.; Loh, K. P. Controllable synthesis of 2D and 1D MoS2 nanostructures on Au surface. *Adv. Funct. Mater.* **2017**, *27*, 1603887.

(17) Byskov, L. S.; Nørskov, J. K.; Clausen, B. S.; Topsøe, H. DFT calculations of unpromoted and promoted MoS2-based hydrodesulfurization catalysts. *J. Catal.* **1999**, *187*, 109–122.

(18) Sharifvaghefi, S.; Yang, B.; Zheng, Y. New insights on the role of H2S and sulfur vacancies on dibenzothiophene hydrodesulfurization over MoS2 edges. *Appl. Catal., A* **2018**, *566*, 164–173.

(19) Raybaud, P.; Hafner, J.; Kresse, G.; Kasztelan, S.; Toulhoat, H. Ab initio study of the H2–H2S/MoS2 gas–solid interface: The nature of the catalytically active sites. *J. Catal.* **2000**, *189*, 129–146.

(20) Bollinger, M. V.; Jacobsen, K. W.; Nørskov, J. K. Atomic and electronic structure of MoS 2 nanoparticles. *Phys. Rev. B* **2003**, *67*, 085410.

(21) Cristol, S.; Paul, J. F.; Payen, E.; Bougeard, D.; Clémendot, S.; Hutschka, F. Theoretical study of the MoS2 (100) surface: a chemical potential analysis of sulfur and hydrogen coverage. *J. Phys. Chem. C* **2000**, *104*, 11220–11229.

(22) Lauritsen, J.; Nyberg, M.; Nørskov, J. K.; Clausen, B.; Topsøe, H.; Lægsgaard, E.; Besenbacher, F. Hydrodesulfurization reaction pathways on MoS2 nanoclusters revealed by scanning tunneling microscopy. *J. Catal.* **2004**, *224*, 94–106.

(23) Lauritsen, J. V.; Kibsgaard, J.; Helveg, S.; Topsøe, H.; Clausen, B. S.; Lægsgaard, E.; Besenbacher, F. Size-dependent structure of MoS 2 nanocrystals. *Nat. Nanotechnol.* **2007**, *2*, 53–58.

(24) Helveg, S.; Lauritsen, J. V.; Lægsgaard, E.; Stensgaard, I.; Nørskov, J. K.; Clausen, B. S.; Topsøe, H.; Besenbacher, F. Atomic-scale structure of single-layer MoS 2 nanoclusters. *Phys. Rev. Lett.* **2000**, *84*, 951.

(25) Bruix, A.; Füchtbauer, H. G.; Tuxen, A. K.; Walton, A. S.; Andersen, M.; Porsgaard, S.; Besenbacher, F.; Hammer, B.; Lauritsen, J. V. In situ detection of active edge sites in single-layer MoS2 catalysts. *ACS nano* **2015**, *9*, 9322–9330.

(26) Grønborg, S. S.; Salazar, N.; Bruix, A.; Rodríguez-Fernández, J.; Thomsen, S. D.; Hammer, B.; Lauritsen, J. V. Visualizing hydrogen-induced reshaping and edge activation in MoS 2 and Co-promoted MoS 2 catalyst clusters. *Nat. Commun.* **2018**, *9*, 1–11.

(27) Mom, R. V.; Louwen, J. N.; Frenken, J. W. M.; Groot, I. M. N. In situ observations of an active MoS 2 model hydrodesulfurization catalyst. *Nat. Commun.* **2019**, *10*, 1–8.

(28) Hinnemann, B.; Moses, P. G.; Bonde, J.; Jørgensen, K. P.; Nielsen, J. H.; Horch, S.; Chorkendorff, I.; Nørskov, J. K. Biomimetic hydrogen evolution: MoS2 nanoparticles as catalyst for hydrogen evolution. *J. Am. Chem. Soc.* **2005**, *127*, 5308–5309.

(29) Yan, Y.; Xia, B.; Xu, Z.; Wang, X. Recent development of molybdenum sulfides as advanced electrocatalysts for hydrogen evolution reaction. *ACS Catal.* **2014**, *4*, 1693–1705.

(30) Pumera, M.; Sofer, Z.; Ambrosi, A. Layered transition metal dichalcogenides for electrochemical energy generation and storage. *J. Mater. Chem.A* **2014**, *2*, 8981–8987.

(31) Jaramillo, T. F.; Jørgensen, K. P.; Bonde, J.; Nielsen, J. H.; Horch, S.; Chorkendorff, I. Identification of active edge sites for electrochemical H2 evolution from MoS2 nanocatalysts. *science* **2007**, *317*, 100–102.

(32) Tan, S. M.; Ambrosi, A.; Sofer, Z.; Huber, Š.; Sedmidubskỳ, D.; Pumera, M. Pristine basal-and edge-plane-oriented molybdenite MoS2 exhibiting highly anisotropic properties. *Chem.–Eur. J.* **2015**, *21*, 7170–7178.

(33) Bonde, J.; Moses, P. G.; Jaramillo, T. F.; Nørskov, J. K.; Chorkendorff, I. Hydrogen evolution on nano-particulate transition metal sulfides. *Faraday Discuss.* **2009**, *140*, 219–231.

(34) Tsai, C.; Chan, K.; Abild-Pedersen, F.; Nørskov, J. K. Active edge sites in MoSe 2 and

WSe 2 catalysts for the hydrogen evolution reaction: a density functional study. *Phys. Chem. Chem. Phys.* **2014**, *16*, 13156–13164.

(35) Cheng, C.-C.; Lu, A.-Y.; Tseng, C.-C.; Yang, X.; Hedhili, M. N.; Chen, M.-C.; Wei, K.-H.; Li, L.-J. Activating basal-plane catalytic activity of two-dimensional MoS2 monolayer with remote hydrogen plasma. *Nano Energy* **2016**, *30*, 846–852.

(36) An, Y.-R.; Fan, X.-L.; Luo, Z.-F.; Lau, W.-M. Nanopolygons of monolayer MS2: best morphology and size for HER catalysis. *Nano Lett.* **2017**, *17*, 368–376.

(37) Nørskov, J. K.; Bligaard, T.; Logadottir, A.; Kitchin, J. R.; Chen, J. G.; Pandelov, S.; Stimming, U. Trends in the Exchange Current for Hydrogen Evolution. *J. Electrochem. Soc.* **2005**, *152*, J23.

(38) Parsons, R. The rate of electrolytic hydrogen evolution and the heat of adsorption of hydrogen. *Trans. Faraday Soc.* **1958**, *54*, 1053–1063.

(39) Hansen, L. P.; Ramasse, Q. M.; Kisielowski, C.; Brorson, M.; Johnson, E.; Topsøe, H.; Helveg, S. Atomic-scale edge structures on industrial-style MoS2 nanocatalysts. *Angew. Chem. - Int. Ed.* **2011**, *50*, 10153–10156.

(40) Zhou, W.; Zou, X.; Najmaei, S.; Liu, Z.; Shi, Y.; Kong, J.; Lou, J.; Ajayan, P. M.; Yakobson, B. I.; Idrobo, J.-C. Intrinsic structural defects in monolayer molybdenum disulfide. *Nano Lett.* **2013**, *13*, 2615–2622.

(41) Kronberg, R.; Hakala, M.; Holmberg, N.; Laasonen, K. Hydrogen adsorption on MoS 2-surfaces: A DFT study on preferential sites and the effect of sulfur and hydrogen coverage. *Phys. Chem. Chem. Phys.* **2017**, *19*, 16231–16241.

(42) Huang, Y.; Nielsen, R. J.; Goddard III, W. A.; Soriaga, M. P. The reaction mechanism with free energy barriers for electrochemical dihydrogen evolution on MoS2. *J. Am. Chem. Soc.* **2015**, *137*, 6692–6698.

(43) Ghuman, K. K.; Yadav, S.; Singh, C. V. Adsorption and dissociation of H2O on monolayered MoS2 edges: Energetics and mechanism from ab initio simulations. *J. Phys. Chem. C* **2015**, *119*, 6518–6529.

(44) Abidi, N.; Bonduelle-Skrzypczak, A.; Steinmann, S. N. Revisiting the Active Sites at the MoS2/H2O Interface via Grand-Canonical DFT: The Role of Water Dissociation. *ACS Appl. Mater. Interfaces* **2020**, *12*, 31401–31410.

(45) Mathew, K.; Kolluru, V. S. C.; Mula, S.; Steinmann, S. N.; Hennig, R. G. Implicit self-consistent electrolyte model in plane-wave density-functional theory. *J. Chem. Phys.* **2019**, *151*, 234101.

(46) Abidi, N.; Lim, K. R. G.; Seh, Z. W.; Steinmann, S. N. Atomistic modeling of electrocatalysis: Are we there yet? *WIREs Comput. Mol. Sci.* **2020**, e1499.

(47) Kresse, G.; Furthmüller, J. Efficiency of ab-initio total energy calculations for metals and semiconductors using a plane-wave basis set. *Comput. Mater. Sci.* **1996**, *6*, 15–50.

(48) Perdew, J. P.; Burke, K.; Ernzerhof, M. Generalized gradient approximation made simple. *Phys. Rev. Lett.* **1996**, *77*, 3865.

(49) Steinmann, S. N.; Corminboeuf, C. Comprehensive benchmarking of a density-dependent dispersion correction. *J. Chem. Theory Comput.* **2011**, *7*, 3567–3577.

(50) Steinmann, S. N.; Sautet, P.; Michel, C. Solvation free energies for periodic surfaces: comparison of implicit and explicit solvation models. *Phys. Chem. Chem. Phys.* **2016**, *18*, 31850–31861.

(51) Blochl, P. E. Projector augmented-wave method. *Phys. Rev. B* **1994**, *50*, 17953.

(52) Kresse, G.; Joubert, D. From ultrasoft pseudopotentials to the projector augmented-wave method. *Phys. Rev. B* **1999**, *59*, 1758.

(53) Steinmann, S. N.; Sautet, P. Assessing a first-principles model of an electrochemical interface by comparison with experiment. *J. Phys. Chem. C* **2016**, *120*, 5619–5623.

(54) Steinmann, S. N.; Michel, C.; Schwiedernoch, R.; Sautet, P. Impacts of electrode potentials and solvents on the electroreduction of CO2: A comparison of theoretical approaches. *Phys. Chem. Chem. Phys.* **2015**, *17*, 13949–13963.

(55) Lespes, N.; Filhol, J. S. Using Implicit Solvent in Ab Initio Electrochemical Modeling: Investigating Li+/Li Electrochemistry at a Li/Solvent Interface. *J. Chem. Theory Comput.* **2015**, *11*, 3375–3382.

(56) Hajar, Y. M.; Treps, L.; Michel, C.; Baranova, E. A.; Steinmann, S. N. Theoretical insight into the origin of the electrochemical promotion of ethylene oxidation on ruthenium oxide. *Catal. Sci. Technol.* **2019**, *9*, 5915–5926.

(57) Jinnouchi, R.; Anderson, A. B. Electronic structure calculations of liquid-solid interfaces: Combination of density functional theory and modified Poisson-Boltzmann theory. *Phys. Rev. B* **2008**, *77*, 245417.

(58) Fang, Y.-H.; Liu, Z.-P. Mechanism and Tafel Lines of Electro-Oxidation of Water to Oxygen on RuO2(110). *J. Am. Chem. Soc.* **2010**, *132*, 18214–18222.

(59) Letchworth-Weaver, K.; Arias, T. A. Joint density functional theory of the electrode-electrolyte interface: Application to fixed electrode potentials, interfacial capacitances, and potentials of zero charge. *Phys. Rev. B* **2012**, *86*, 075140.

(60) Sundararaman, R.; Goddard, W. A.; Arias, T. A. Grand canonical electronic density-functional theory: Algorithms and applications to electrochemistry. *J. Chem. Phys.* **2017**, *146*, 114104.

(61) Zhang, H.; Goddard, W. A.; Lu, Q.; Cheng, M.-J. The importance of grand-canonical quantum mechanical methods to describe the effect of electrode potential on the sta-

bility of intermediates involved in both electrochemical CO2 reduction and hydrogen evolution. *Phys. Chem. Chem. Phys.* **2018**, *20*, 2549–2557.

(62) Hörmann, N. G.; Andreussi, O.; Marzari, N. Grand canonical simulations of electrochemical interfaces in implicit solvation models. *J. Chem. Phys.* **2019**, *150*, 041730.

(63) Melander, M. M.; Kuisma, M. J.; Christensen, T. E. K.; Honkala, K. Grand-canonical approach to density functional theory of electrocatalytic systems: Thermodynamics of solid-liquid interfaces at constant ion and electrode potentials. *J. Chem. Phys.* **2019**, *150*, 041706.

(64) Melander, M. M. Grand canonical ensemble approach to electrochemical thermodynamics, kinetics, and model Hamiltonians. *Curr. Opin. Electrochem.* **2021**, 100749.

(65) Curutchet, A.; Colinet, P.; Michel, C.; Steinmann, S. N.; Le Bahers, T. Two-sites are better than one: revisiting the OER mechanism on CoOOH by DFT with electrode polarization. *Phys. Chem. Chem. Phys.* **2020**, *22*, 7031–7038.

(66) Shang, R.; Steinmann, S. N.; Xu, B.-Q.; Sautet, P. Mononuclear Fe in N-doped carbon: computational elucidation of active sites for electrochemical oxygen reduction and oxygen evolution reactions. *Catal. Sci. Technol.* **2020**, *10*, 1006–1014.

(67) Panaritis, C.; Hajar, Y. M.; Treps, L.; Michel, C.; Baranova, E. A.; Steinmann, S. N. Demystifying the Atomistic Origin of the Electric Field Effect on Methane Oxidation. *J. Phys. Chem. Lett.* **2020**, *11*, 6976–6981.

(68) Deubel, D. V.; Lau, J. K.-C. In silico evolution of substrate selectivity: comparison of organometallic ruthenium complexes with the anticancer drug cisplatin. *Chem. Commun.* **2006**, 2451–2453.

(69) Kua, J.; Thrush, K. L. HCN, Formamidic Acid, and Formamide in Aqueous Solution: A Free-Energy Map. *J. Phys. Chem. B* **2016**, *120*, 8175–8185.

(70) Nørskov, J. K.; Rossmeisl, J.; Logadottir, A.; Lindqvist, L. R. K. J.; Kitchin, J. R.; Bligaard, T.; Jonsson, H. Origin of the overpotential for oxygen reduction at a fuel-cell cathode. *J. Phys. Chem. B* **2004**, *108*, 17886–17892.

(71) Tsai, C.; Chan, K.; Nørskov, J. K.; Abild-Pedersen, F. Rational design of MoS 2 catalysts: tuning the structure and activity via transition metal doping. *Catal. Sci. Technol.* **2015**, *5*, 246–253.

(72) Tsai, C.; Chan, K.; Nørskov, J. K.; Abild-Pedersen, F. Theoretical insights into the hydrogen evolution activity of layered transition metal dichalcogenides. *Surf. Sci.* **2015**, *640*, 133–140.

(73) Kibsgaard, J.; Tsai, C.; Chan, K.; Benck, J. D.; Nørskov, J. K.; Abild-Pedersen, F.; Jaramillo, T. F. Designing an improved transition metal phosphide catalyst for hydrogen evolution using experimental and theoretical trends. *Energy Environ. Sci.* **2015**, *8*, 3022–3029.

Graphical TOC Entry